Research Square

Preprints are preliminary reports that have not undergone peer review.
They should not be considered conclusive, used to inform clinical practice,
or referenced by the media as validated information.

AI-Based Low-Dose Chest CT Assessment of Coronary Artery Calcification Score: An Analysis of Accuracy-Relating Factors

Xiao Juan Lin
Fujian Medical University School of Medical Imaging
Bo Rong Tang
Fujian Medical University School of Medical Imaging
Lin Sha Cai
Fujian Medical University School of Medical Imaging
Li Wei Xue
Fujian Medical University Union Hospital
Li Li Wang
Fujian Medical University Union Hospital
Wan Yi Zheng
Fujian Medical University Union Hospital
Su Ping Chen
CT Imaging research center, GE HealthCare
Xiong Xin Ye
Fujian Medical University Union Hospital
Yun Jing Xue
Fujian Medical University Union Hospital
Yuan Fen Liu
15692054@qq.com

Fujian Medical University Union Hospital

Research Article

Keywords: cardiac CT, chest CT, CACS, artificial intelligence, coronary heart disease

Posted Date: March 28th, 2026

DOI: https://doi.org/10.21203/rs.3.rs-8352702/v1

License: This work is licensed under a Creative Commons Attribution 4.0 International License. Read Full License

Additional Declarations: No competing interests reported.

Abstract

Objective: This study aimed to assess the accuracy of AI-based coronary artery calcium scoring on non-gated low-dose chest CT and to identify factors influencing calcium risk classification, using ECG-gated non-contrast cardiac CT as the reference standard.

Methods: A total of 312 patients with chest pain were prospectively included and underwent ECG-gated non-contrast cardiac CT plus an additional low-dose chest CT. Images from the low-dose chest CT were reconstructed using both a lung kernel and a standard reconstruction kernel. AI software automatically generated coronary artery calcium scores (Agatston, mass, volume and total CACS) on both scan types. Patients were stratified by Agatston-based calcium risk, heart rate (≤ / > 65 bpm) and BMI (< / ≥ 25 kg/m²). Agreement and systematic bias between non-gated low-dose CACS and the reference ECG-gated CACS were evaluated with paired tests and linear regression, and confusion matrices were used to assess risk-stratification performance in each subgroup and HR–BMI combination.

Results: Pulmonary-kernel LDCT yielded Agatston scores consistent with ECG-gated CT, without significant differences across heart-rate, BMI, or calcium-severity subgroups. Under the pulmonary kernel, measurement bias was weakly but significantly correlated with heart rate and BMI ($r = 0.145$, $r = 0.131$; both $P < 0.05$). Overall, CACS derived from non-gated low-dose chest CT showed excellent correlation with the reference standard ($r > 0.94$). The low-HR/low-BMI subgroup achieved the best performance for calcium risk stratification, with 80% accuracy and good agreement ($\kappa = 0.72$).

Conclusion: Reconstruction kernel, heart rate, BMI, and calcium severity significantly influence the accuracy of AI-based CACS derived from non-gated low-dose chest CT. Compared with standard reconstruction, the pulmonary kernel provides more accurate calcium scoring and better coronary artery disease risk stratification, particularly in patients with low heart rate and low BMI. Integrating AI-based coronary calcium assessment into low-dose chest CT for lung cancer screening is feasible, offering dual benefits from a single scan and supporting early cardiovascular disease prevention.

Trial registration: Chinese Clinical Trial Registry (2025.04.02, ChiCTR2500100073)

Background

Coronary artery calcium score (CACS) is an established biomarker of subclinical atherosclerosis and a strong predictor of coronary heart disease risk. Accurate quantification of CACS is therefore essential for early risk stratification and timely intervention[1–3]. The guideline-recommended standard for CACS assessment, electrocardiography (ECG)-gated non-contrast cardiac CT, provides reliable measurements and is particularly valuable in symptomatic patients with chest pain[4]. However, the incremental benefit of performing an additional ECG-gated non-contrast CT solely for screening is limited by concerns regarding radiation exposure. In contrast, low-dose chest CT(LDCT) for lung cancer screening, which has been endorsed by multiple guidelines, inherently covers the heart and great vessels. This enables CACS assessment without extra radiation dose or scan time and may provide an opportunity for large-scale early risk screening for coronary artery disease[4,5].

With the incidental detection of CACS on LDCT for lung cancer screening, many studies have suggested routinely including CACS in these reports. However, such additional reporting would inevitably increase the workload for radiologists[6–8]. In parallel, rapid advances in artificial intelligence (AI) in medical imaging have shown that AI-

automated CACS closely agrees with manual analysis and demonstrates good reproducibility, thereby substantially reducing processing time and inter-observer variability[9,10].

When CACS is derived from non-gated LDCT rather than ECG-gated cardiac CT, additional sources of error must be considered. Elevated heart rate can exacerbate motion artefacts and lead to underestimation of calcifications; increased BMI may degrade image quality and similarly result in underestimation; and differences in edge enhancement and noise suppression among reconstruction algorithms can further affect calcification detection[11,12]. Although several studies have evaluated the agreement between non-ECG-gated LDCT–derived CACS and standard ECG-gated cardiac CT in terms of quantitative scores and risk stratification, they have typically focused on single factors such as heart rate, BMI, slice thickness, or scanning technique[13,14]. For AI-based CACS on non-gated LDCT. However, most existing work remains limited to reporting overall correlation or agreement with ECG-gated cardiac CT as the reference standard. Systematic and comprehensive quantitative analyses of measurement bias relative to this standard, as well as risk stratification accuracy under the influence of multiple factors (heart rate, BMI, reconstruction parameters, and calcium severity) and their interactions, are still scarce.

Therefore, this study aimed to systematically evaluate, under different reconstruction kernels, the agreement between AI-based CACS derived from non-gated LDCT and those obtained from ECG-gated non-contrast cardiac CT as the reference standard. In addition, we investigated the effects of heart rate and BMI, both individually and in combination, on measurement bias and the diagnostic performance of calcium risk stratification, with the goal of informing clinical application in different patient subgroups.

Methods

Study Participate

The institutional review board approved this prospective, single-center investigation, and each participant provided written informed consent. We screened consecutive patients who presented to our hospital with chest pain from December 2024 through March 2025. Patients were eligible if clinicians ordered coronary CT angiography (CCTA) together with an ECG-gated non-contrast cardiac CT (SD-ECG cardiac CT) for Agatston coronary artery calcium scoring. As part of the study protocol, all included participants also underwent a non-gated low-LDCT before the cardiac CT acquisitions. Inclusion criteria were chest-pain presentation during the enrollment window and the need for both SD-ECG cardiac CT and CCTA to assess coronary calcification. Exclusion criteria comprised (1) a history or imaging findings consistent with prior coronary artery bypass grafting or percutaneous coronary intervention; (2) the presence of a mechanical valve, other implanted cardiac devices, or congenital coronary artery hypoplasia; and (3) inability to perform adequate breath-holding or scans degraded by marked respiratory motion artifacts. Ultimately, 312 patients met the criteria and were enrolled (Fig. 1).

CT Image Acquisition

All examinations were performed on a 256-slice CT system (Revolution CT, GE Healthcare). We positioned patients supine with their arms raised above the head and used voice prompts to instruct breath-holding during image acquisition. For ECG-gated non-contrast cardiac CT for calcium scoring (SD-ECG cardiac CT), we applied the following acquisition settings: tube voltage of 120 kVp; automatic tube current modulation (noise index, 20.0; tube current range, 50–430 mA); gantry rotation time of 0.28 s; and prospective ECG triggering at 75% of the R–R interval. Coverage extended from the tracheal carina to the cardiac apex. We reconstructed images with a standard kernel at

2.5-mm slice thickness using 50% ASiR-V. For non-gated LDCT, we used 120 kVp with automatic tube current modulation (noise index, 22.0; tube current range, 10–570 mA), a gantry rotation time of 0.5 s, and a scan range from the lung apices to 2–3 cm below the diaphragm. We reconstructed LDCT images using both standard and lung kernels at 2.5-mm slice thickness with 50% ASiR-V. We recorded the volumetric CT dose index (CTDIvol) for both protocols.

CACS Score Calculation

All images were evaluated using an AI-based automated CACS software (Shu kun Technology, China). For each patient, either non-gated LDCT or ECG-gated non-contrast cardiac CT images were first imported into the software. The images then underwent preprocessing, including filtering and noise reduction, to improve overall image quality. A convolutional neural network was used to automatically segment the heart and delineate the individual coronary artery branches. Candidate calcified lesions in each coronary artery were identified by applying a fixed attenuation threshold (> 130 HU) and a minimum area criterion (≥ 1 mm^2) using thresholding and connected-component analysis[15]. After calcified regions were detected, the Agatston score was calculated by assigning a density factor according to the maximum CT attenuation within each lesion (130–199 HU = 1, 200–299 HU = 2, 300–399 HU = 3, ≥ 400 HU = 4) and multiplying this factor by the lesion area. Incorporating image parameters (CT attenuation, area, volume, and slice thickness), the algorithm automatically generated vessel-specific and total CACS, including scores for the left main coronary artery (LM), left anterior descending artery (LAD), left circumflex artery (LCX), right coronary artery (RCA), and the overall sum. Risk stratification was performed according to the CAC-DRS classification as follows: no calcification (CACS = 0), mild calcification (CACS 1–99), moderate calcification (CACS 100–399), and severe calcification (CACS ≥ 400). Volume scores and mass scores were computed simultaneously[4,16].

The model was trained on a large dataset of matched ECG-gated and non-gated CT examinations. By leveraging these paired studies, the deep learning algorithm learned to recognize imaging signatures of coronary artery calcification on non-gated CT, allowing accurate detection and quantification of coronary calcium on non-gated LDCT scans. A separate tuning (validation) set was used during training to optimize the model and further improve its accuracy and generalizability[17].

Data Analysis

Statistical analyses used SPSS version 26.0 (IBM Corp., Armonk, NY, USA), and figures were created in GraphPad Prism (GraphPad Software, San Diego, CA, USA). Because continuous variables were not normally distributed, data are reported as the median and interquartile range (IQR; 25th–75th percentile). The Wilcoxon signed-rank test compared CACS from ECG-gated standard cardiac CT with CACS derived from non-gated LDCT reconstructed with different kernels. Linear regression was performed to evaluate the relationship between LDCT-based CACS and the reference standard and to examine associations between measurement bias and heart rate, BMI, and coronary calcium severity. Confusion matrices and Cohen's kappa were used to assess the accuracy and agreement of calcium risk stratification across subgroups and subgroup combinations. A two-sided P value < 0.05 was considered statistically significant.

Results

Patient characteristics

Patient characteristics are summarized in Table 1. Overall, 312 patients were included, including 128 men, with a mean age of 64.98 ± 11.50 years (range, 36–93 years). The CTDIvol was significantly higher for SD-ECG cardiac CT than for non-gated LDCT (2.96 ± 0.91 vs 1.79 ± 0.39; P < 0.001).

Table 1
Patient characteristics

Characteristics	Value
Female (n %)	128(41%)
Age (years, Mean ± SD)	64.98 ± 11.50
Hate Rate	
≤ 65 bpm	75(24%)
>65	237(76%)
BMI	
<25 kg/m^2	205(65.7%)
≥ 25 kg/m^2	107(34.3%)
Agatston Grade	
No	100(32%)
Mild	109(35%)
Moderate	69(22%)
Severe	34(11%)

Comparison and Correlation Analysis of Calcification Scores Between Non-gated LDCT and Gated Cardiac CT

Table 2 summarizes artery-specific and total CACS obtained with both protocols. For total calcium burden, volume- and mass-based scores from non-gated LDCT differed significantly from those measured on SD-ECG cardiac CT. In contrast, Agatston scores from LDCT reconstructed with the lung kernel were not significantly different from the SD-ECG cardiac CT reference, whereas Agatston scores from LDCT reconstructed with the standard kernel showed a significant difference. Overall, both LDCT reconstructions tended to underestimate calcification relative to the reference standard, with greater underestimation observed for the standard-kernel reconstruction than for the lung-kernel reconstruction.

Despite these differences, calcium scores derived from LDCT and ECG-gated cardiac CT were highly correlated. Scatter plots demonstrated very strong linear correlations (r > 0.94, P < 0.001) between LDCT-derived and SD-ECG–cardiac CT–derived values for all three metrics—mass score, volume score, and Agatston score (Fig. 4).

Comparison of Calcification Scores Between Non-Gated LDCT and Gated Cardiac CT Under Stratification by Heart Rate, BMI, and Calcification Severity

When stratified by heart rate, LDCT images reconstructed with the lung kernel showed no statistically significant differences in Agatston scores compared with SD-ECG–cardiac CT in either the low- or high-HR subgroup ($P > 0.05$), whereas the corresponding volume and mass scores remained significantly lower than the reference standard ($P < 0.05$). In contrast, for LDCT reconstructed with the standard kernel, all three calcium metrics (Agatston, volume, and mass scores) differed significantly from the reference standard in both heart rate subgroups ($P < 0.05$), while the degree of underestimation did not differ significantly between low- and high-HR groups (Table 3).

BMI-stratified analyses showed a similar pattern. With lung-kernel reconstruction, LDCT-derived Agatston scores were comparable to those from SD-ECG cardiac CT across BMI subgroups ($P > 0.05$), whereas volume and mass scores remained consistently and significantly different from the reference standard ($P < 0.05$). With standard-kernel reconstruction, all three CAC metrics differed significantly from the reference standard ($P < 0.05$). Measurement bias did not differ significantly between the low- and high-BMI groups (Table 3).

Across calcification risk categories, both lung- and standard-kernel LDCT reconstructions showed no significant difference from the reference standard in the no-calcification group (CACS = 0; $P > 0.05$). In calcified patients, lung-kernel reconstructions yielded Agatston scores that did not differ significantly from SD-ECG–cardiac CT in the mild, moderate, or severe calcification subgroups (all $P > 0.05$). However, lung-kernel mass scores were significantly lower than the reference standard across all three risk categories ($P < 0.05$), and volume scores differed significantly only in the mildly calcified group. For standard-kernel reconstructions, both Agatston and mass scores were significantly different from the reference standard in all three calcification severity subgroups ($P < 0.05$), and volume scores also differed significantly in the mild and moderate calcification groups (Table 3).

Table 2
Sign rank test analysis of non-gated LDCT and ECG-gated cardiac CT under different reconstruction algorithms

	SD-ECG-Cardiac (STND)	LDCT-non-ECG Lung kernel	LDCT-non-ECG Standard kernel	P1 value	P2 value
Volume					
Total	30.95(0,159.29)	21.33(0,139.66)	15.71(0,124.26)	< 0.001	< 0.001
LM	0(0,0)	0(0,0)	0(0,0)	< 0.001	0.15
LAD	12.82(0,66.79)	8.38(0,72.69)	2.14(0,58.20)	0.461	< 0.001
LCX	0(0,11.62)	0(0,0)	0(0,0)	< 0.001	< 0.001
RCA	0(0,17.79)	0(0,14.77)	0(0,10)	0.724	< 0.001
Mass					
Total	5.53(0,34.98)	6.41(0,41.44)	2.18(0,23)	< 0.001	< 0.001
LM	0(0,0)	0(0,0)	0(0,0)	0.06	0.007
LAD	2.13(0,14.56)	2.49(00,23.05)	0.26(0,11.09)	< 0.001	< 0.001
LCX	0(0,1.75)	0(0,0)	0(0,0)	0.045	< 0.001
RCA	0(0,3.03)	0(0,3.67)	0(0,1.34)	< 0.001	< 0.001
Agaston					
Total	30.13(0,176.29)	29.49(0,184.73)	10(0,125.69)	0.291	< 0.001
LM	0(0,0)	0(0,0)	0(0,0)	< 0.001	0.032
LAD	11.19(0,75.99)	10.82(0,94.73)	0.72(0,61.65)	0.009	< 0.001
LCX	0(0,9.76)	0(0,0)	0(0,0)	0.069	< 0.001
RCA	0(0,15.68)	0(0,17.64)	0(0,6.67)	0.08	< 0.001

The P1 value represents the analysis result between SD-ECG-Cardiac CT and LDCT-non-ECG-Lung kernel, The P2 value represents the analysis result between SD-ECG-Cardiac CT and LDCT-non-ECG-Standard kernel.

Table 3
Analysis of the symbol rank sum test between non-gated LDCT and ECG-gated cardiac CT under different subgroups

	SD-ECG-Cardiac	LDCT-non-ECG Lung kernel	LDCT-non-ECG Standard kernel	P1 value	P2 value
HR Subgroup					
HR ≤ 65					
Volume	17.29(0, 116.23)	11.43(0,88.55)	10.00(0,82.84)	0.005	0.014
Mass	3.16(0, 30.42)	3.29(0,35.95)	1.4(0,15.44)	0.006	< 0.001
Agaston	20.66(0,146.03)	14.28(0,114.26)	6.67(0,84.74)	0.186	< 0.001
HR>65					
Volume	38.74(0,167.04)	24.92(0,162.12)	18.57(0,147.11)	0.016	< 0.001
Mass	5.89(0,35.89)	7.17(,49.99)	2.18(0,26.78)	< 0.001	< 0.001
Agaston	35.57(0,190.67)	33.33(0,214.01)	12.85(0,147.35)	0.068	< 0.001
BMI Subgroup					
BMI < 25					
Volume	29.80(0,157.26)	17.23(0,160.67)	15.74(0,155.69)	0.013	< 0.001
Mass	5.22(0,37.18)	5.40(0,50.48)	2.10(0,29.25)	< 0.001	< 0.001
Agaston	29.8(0,177.18)	20.95(0.207.44)	9.52(0,152.93)	0.777	< 0.001
BMI ≥ 25					
Volume	38.74(0,169.97)	27.14(0,125.69)	15.71(0,87.13)	0.03	< 0.001
Mass	5.84(0,30.74)	8.03(0.33.39)	2.96(0,16.05)	< 0.001	< 0.001
Agaston	32.00(0,165.10)	34.41(0,154.11)	12.85(0,83.79)	0.159	< 0.001
CACS Subgroup					
No calcification					
Volume	0(0,0)	0(0,0)	0(0,0)	0.66	0.18

	SD-ECG-Cardiac	LDCT-non-ECG Lung kernel	LDCT-non-ECG Standard kernel	P1 value	P2 value
HR Subgroup					
HR ≤ 65					
Mass	0(0,0)	0(0,0)	0(0,0)	0.66	0.18
Agaston	0(0,0)	0(0,0)	0(0,0)	0.66	0.18
Mild calcification					
Volume	29.80(14.01,55.39)	19.45(1.54,43.57)	14.28(0,42.85)	0.002	< 0.001
Mass	5.26(2.16,10.32)	6.13(0.45,15.13)	2.10(0,7.29)	< 0.001	< 0.001
Agaston	29.80(11.57,57.89)	27.4(2.05,56.89)	10.00(0,35.47)	0.489	< 0.001
Moderate calcification					
Volume	178.76(127.02)	182.38(112.12,236.60)	159.97(94.98,227.10)	0.149	0.002
Mass	39.70(27.02,57.37)	55.57(35.08,76.18)	32.15(16.99,42.71)	< 0.001	< 0.001
Agaston	208.18(143.95,298.70)	235.43(147.12,301.99)	208.18(94.51,249.46)	0.169	< 0.001
Severe calcification					
Volume	622.62(398.68,947.72)	572.45(381.77,888.77)	578.465(396.00,809.85)	0.158	0.164
Mass	147.295(91.59,289.97)	193.25(121.13,306.21)	109.28(69.83,178.46)	0.002	< 0.001
Agaston	775.95(471.02,1248.14)	753.02(498.00,1143.22)	623.69(375.97,957.09)	0.925	0.005

The P1 value represents the analysis result between SD-ECG-Cardiac CT and LDCT-non-ECG-Lung kernel, The P2 value represents the analysis result between SD-ECG-Cardiac CT and LDCT-non-ECG-Standard kernel.

Analysis of Error Factors

With lung-kernel reconstruction, Agatston score error showed weak but statistically significant linear correlations with heart rate ($r = 0.145$, $P = 0.011$) and BMI ($r = 0.131$, $P = 0.021$). By contrast, with standard-kernel reconstruction, the associations between Agatston score error and either heart rate or BMI were not significant (all $P > 0.05$). Likewise, volume- and mass-score errors were not significantly correlated with heart rate or BMI for either reconstruction kernel (all $P > 0.05$).

For all three calcium metrics (Agatston, volume, and mass scores), measurement errors from the standard-kernel reconstruction were strongly correlated with the corresponding reference calcification scores (all $P < 0.001$). Under the lung-kernel reconstruction, only mass-score error showed a statistically significant correlation with the corresponding calcification scores ($P < 0.001$). Because heart rate and BMI exerted heterogeneous effects on measurement error in the lung-kernel reconstructions and global calibration models failed to improve overall diagnostic performance, subgroup analyses were subsequently performed to assess whether heart rate and BMI influenced the accuracy of calcification risk stratification (Fig. 2).

Efficacy Analysis of Overall Calcification Risk Stratification

In the overall analysis of calcification risk stratification, both lung-kernel and standard-kernel LDCT reconstructions demonstrated good diagnostic accuracy compared with the reference standard. The lung-kernel reconstruction slightly outperformed the standard kernel, with an overall accuracy of 80.12% for risk stratification; 23 cases (7.37%) were overestimated by one risk category and 39 cases (12.50%) were underestimated by one category, and all misclassifications occurred only between adjacent risk categories. For the standard-kernel reconstruction, the overall accuracy of risk stratification was 79.48%, with 6 cases (1.92%) overestimated and 58 cases (18.59%) underestimated by one category, again with no misclassification exceeding a single risk category. Cohen's kappa coefficients for risk stratification indicated good agreement for both reconstruction kernels, with $\kappa = 0.72$ for the lung kernel and $\kappa = 0.71$ for the standard kernel (Fig. 5).

Analysis of Diagnostic Results in Subgroups

Because only Agatston score errors derived from LDCT under the pulmonary kernel showed significant correlations with BMI and heart rate, efficacy analyses for calcification risk stratification were performed in HR and BMI subgroups for the pulmonary-kernel LDCT data (Fig. 3). No significant difference in the overall accuracy of risk stratification was observed between the low- and high-BMI groups (ACC: 80.00% vs 80.37%). In contrast, diagnostic performance was better in the low-HR group than in the high-HR group (ACC: 84.00% vs 78.90%).

However, the diagnostic performance of pulmonary-kernel LDCT for calcification risk stratification varied across different combinations of HR and BMI (Table 4). The combination of low HR and low BMI yielded the best performance (ACC = 84.61%, PPV = 88.01%, TPR = 89.88%, F1-score = 88.94%). In the low-HR and high-BMI subgroup, performance was slightly reduced (ACC = 82.60%, PPV = 85.72%, TPR = 86.05%, F1-score = 85.88%). Among patients with high HR, both BMI subgroups showed lower performance than the corresponding low-HR subgroups: in the high-HR and low-BMI group, ACC was 78.43%, PPV 76.98%, TPR 77.12%, and F1-score 77.05%; in the high-HR and high-BMI group, ACC was 79.76%, PPV 82.40%, TPR 80.11%, and F1-score 81.24%. Overall, these findings suggest that, under pulmonary-kernel LDCT, heart rate has a greater impact on the accuracy of calcification risk stratification than BMI.

Table 4
Analysis of the diagnostic performance of calcification scores in combined subgroups

Subgroup	ACC(%)	PPV(%)	TPR(%)	F1-Score(%)
HR↓+BMI↓	84.61	88.01	89.88	88.94
HR↓+BMI↑	82.60	85.72	86.05	85.88
HR↑+BMI↓	78.43	76.98	77.12	77.05
HR↑+BMI↑	79.76	82.40	80.11	81.24

'↓' represents the low subgroup, '↑' represents the high subgroup. ACC represents the accuracy of diagnostic performance, PPV represents precision, TPR represents recall, and F1-score is the harmonic function of PPV and TPR

Discussion

Regarding the choice of reconstruction kernel for CACS on LDCT, current guidelines recommend using standard reconstruction kernels on ECG-gated non-contrast cardiac CT[4]. However, our findings suggest that, when applied to non-gated LDCT, lung-kernel reconstructions provide better agreement with gated cardiac CT than standard-kernel reconstructions for the calculation of coronary calcium scores. As expected, calcium scores derived from LDCT show some measurement error compared with those from conventional ECG-gated cardiac CT, yet they remain strongly correlated with the reference standard, and the overall diagnostic performance for risk stratification is characterized by high accuracy and good agreement. In the error analysis, heart rate and BMI were positively and significantly correlated with Agatston score errors under the lung-kernel reconstruction. For pulmonary-kernel LDCT, no significant differences in Agatston-based risk stratification accuracy were observed across BMI subgroups, whereas the low-HR subgroup demonstrated better risk stratification performance than the high-HR subgroup. In combined subgroup analyses, the best diagnostic performance was observed in patients with heart rate ≤ 65 bpm and BMI < 25 kg/m², and heart rate appeared to exert a stronger influence on diagnostic performance than BMI when comparing corresponding HR–BMI combinations. These results suggest that LDCT is particularly suitable for AI-based CACS in patients with lower heart rates, especially those with both low HR and low BMI. Taken together, this study indicates that LDCT can be used not only for lung cancer screening but also for opportunistic cardiovascular risk assessment when combined with AI-based CACS, thereby providing dual benefits from a single examination and a feasible imaging pathway for integrated screening in clinical practice.

In this study, AI-based quantitative analysis of ECG-gated non-contrast cardiac CT was used as the reference standard, which differs from most previous studies that relied on manually measured ECG-gated calcium scores as the gold standard. This choice is supported by accumulating evidence that AI software can efficiently process large datasets, maintain consistent algorithms across experimental and control groups, and provide objective and highly reproducible measurements, thereby minimizing observer-related bias from manual segmentation[10,18,19]. Nonetheless, compared with AI-derived CACS from ECG-gated cardiac CT, calcium scores obtained from non-gated LDCT still exhibit systematic deviations, including underestimation of risk categories, misclassification, false positives, and false negatives. Multiple studies have also shown that different image acquisition and reconstruction strategies can introduce similar types of error[12,20].

Several mechanisms may account for these discrepancies. (1) Cardiac motion–related artefacts and partial volume effects: Because ungated LDCT is acquired without ECG synchronization, coronary calcifications may appear blurred, displaced, or partially averaged across slices, leading to inconsistent morphology and lesion size and thus to systematic bias. Consistent with this, subgroup analysis showed that heart rate had a greater impact on diagnostic accuracy than BMI, and represented a major source of systematic error[21–23]. (2) Low-dose–related image noise and motion: Under low-dose conditions, cardiac motion and increased noise degrade image quality and obscure the boundaries and peak attenuation of coronary calcifications, making precise quantification more challenging[23,24]. (3) Body habitus and image noise: Higher BMI is associated with increased noise and artefacts, which may obscure small calcifications or alter their measured density and area, leading to underestimation or instability of the integral scores. Although error analysis under the pulmonary kernel showed a significant correlation between BMI and Agatston errors, BMI had only a modest impact on diagnostic accuracy, and its influence was negligible in the setting of high heart rates[11,25]. (4) Reconstruction algorithms and slice thickness: Prior work has demonstrated that iterative reconstruction, deep learning reconstruction, and different smoothing or sharpening kernels can alter lesion edges and density distributions, thereby affecting both area and density components of the Agatston score. The differences in CACS among reconstruction kernels observed in our study are likely related to these effects. The lung kernel, with its inherently higher spatial resolution, provided better accuracy and consistency for calcium stratification in intermediate-to-high risk groups than the standard kernel; however, the associated increase in image noise made it more prone to overestimating risk compared with the standard kernel[26–28]. (5) Effect of calcification burden: In line with previous studies, we found that at low calcium burdens, missed or underestimated lesions may lead to false negatives and downward risk reclassification, whereas at high burdens, absolute differences and variability relative to the reference standard increase, which can also result in misclassification. Diagnostic accuracy was higher at moderate-to-high calcium loads than at very low loads, likely because greater calcium burden improves lesion conspicuity and contrast, while low-burden disease is more susceptible to noise and motion artefacts that obscure small foci of calcification[29].

In previous studies, Yu et al. used AI software to quantify CACS and assess their regional distribution on chest CT scans[30]. Kim et al. evaluated the consistency and diagnostic performance of LDCT–derived coronary calcium scores across multiple datasets using the DL-CACS system[10]. Although both studies demonstrated good reliability, they did not further characterize potential sources of error or assess the applicability of these methods across different patient subgroups. Beker et al. investigated the impact of heart rate and BMI on CACS derived from virtual non-contrast (VNC) images obtained with photon-counting detector CT (PCD-CT)[31]. Building on this prior work, our study uses non-gated LDCT to derive CACS and goes beyond univariate analyses of HR and BMI. We further evaluate the diagnostic performance of combined HR–BMI subgroups, thereby providing a more systematic assessment of the practical clinical utility of non-gated LDCT for coronary calcium scoring in real-world populations.

Several limitations should be acknowledged. First, because this was a single-center study, both the cohort size and the representation of CAC risk strata may not reflect broader clinical populations, underscoring the need for validation in larger, multicenter datasets. Second, we did not evaluate additional sources of variability—such as different reconstruction approaches (including deep learning–based methods) and dose-related effects—which remain important directions for future work.

Conclusion

In summary, although AI-based CACS derived from non-gated LDCT differ from those obtained with conventional ECG-gated cardiac CT, they still provide high diagnostic accuracy and good agreement for calcification risk

stratification. The accuracy of AI-based CACS from non-gated LDCT is influenced by reconstruction kernel, heart rate, BMI, and the severity of calcification. Among these, pulmonary-kernel reconstructions offer the best performance for coronary heart disease risk stratification, particularly in patients with both low heart rate and low BMI.

Abbreviations

CACS coronary artery calcium score

LDCT non-gated low-dose chest CT

ECG electrocardiography

AI artificial intelligence

HR heart rate

BMI body mass index

SD-ECG- cardiac CT non-enhanced ECG-gated cardiac CT

LM left main coronary artery

LAD left anterior descending artery

LCX left circumflex artery

RCA right coronary artery

CTDIvol Computed Tomography Dose Index - Volume

Declarations

Ethics approval and consent to participate

This study was conducted in accordance with the Declaration of Helsinki. The protocol was approved by the Institutional Ethics Committee of Union Hospital, Fujian Medical University (Approval No. 2025KY007), and written informed consent was obtained from all participants

Consent for publication

Not applicable

Availability of data and materials

The datasets used and/or analyzed during the current study are available from the corresponding author on reasonable request.

Competing interests

Not applicable

Funding

Medical Imaging Specialty Competency Improvement Hospital Management Funding（No.14008021）;Supported by Fujian Provincial Natural Science Foundation of China（No.2025J01133921）

Authors' contributions

XJL contributed to the conception and design of the study, data analysis and interpretation, and drafting of the manuscript. BRT contributed to data analysis and drafting of the manuscript. LSC and LWX contributed to data acquisition. LLW and WYZ contributed to data interpretation and critical revision of the manuscript. SPC contributed to the conception and design of the study, data interpretation, and critical revision of the manuscript. XXY contributed to data acquisition and interpretation. YJX contributed to the conception and design of the study and critical revision of the manuscript. YFL supervised the study and contributed to the conception and design, data interpretation, and critical revision of the manuscript. All authors read and approved the final version of the manuscript.

Acknowledgements

This work was supported by the hospital-managed fund for specialty capacity improvement of the Department of Medical Imaging (Grant No. 14008021) and Fujian Provincial Natural Science Foundation of China (Grant No. 2025J01133921).

Authors' detail:

[1]College of Medical Imaging, Fujian Medical University.[2]Department of Radiology, Union Hospital, Fujian Medical University.[3]CT Imaging research center, GE HealthCare

References

1. Detrano R, Guerci AD, Carr JJ, Bild DE, Burke G, Folsom AR, et al. Coronary calcium as a predictor of coronary events in four racial or ethnic groups. N Engl J Med. 2008;358:1336-45. doi:10.1056/NEJMoa072100.
2. McClelland RL, Jorgensen NW, Budoff M, Blaha MJ, Post WS, Kronmal RA, et al. 10-year coronary heart disease risk prediction using coronary artery calcium and traditional risk factors: derivation in the MESA (Multi-Ethnic Study of Atherosclerosis) with validation in the HNR (Heinz Nixdorf Recall) study and the DHS (Dallas Heart Study). J Am Coll Cardiol. 2015;66:1643-53. doi:10.1016/j.jacc.2015.08.035.
3. Blaha MJ, Whelton SP, Al Rifai M, Dardari Z, Shaw LJ, Al-Mallah MH, et al. Comparing risk scores in the prediction of coronary and cardiovascular deaths: Coronary Artery Calcium Consortium. JACC Cardiovasc Imaging. 2021;14:411-21. doi:10.1016/j.jcmg.2019.12.010
4. Hecht HS, Cronin P, Blaha MJ, Budoff MJ, Kazerooni EA, Narula J, et al. 2016 SCCT/STR. guidelines for coronary artery calcium scoring of noncontrast noncardiac chest CT scans: a report of the Society of Cardiovascular Computed Tomography and Society of Thoracic Radiology. J Cardiovasc Comput Tomogr. 2017;11:74-84. doi:10.1016/j.jcct.2016.11.003.

5. Arnett DK, Blumenthal RS, Albert MA, Buroker AB, Goldberger ZD, Hahn EJ, et al. 2019 ACC/AHA guideline on the primary prevention of cardiovascular disease: a report of the American College of Cardiology/American Heart Association Task Force on Clinical Practice Guidelines. Circulation. 2019;140:e596-646. doi:10.1161/CIR.0000000000000678.
6. Dyer DS, White C, Conley Thomson C, Gieske MR, Kanne JP, Chiles C, et al. A quick reference guide for incidental findings on lung cancer screening CT examinations. J Am Coll Radiol. 2023;20:162-72. doi:10.1016/j.jacr.2022.08.009.
7. Caires MC, Kasuku KM, Mengesha B, Garuba H, Law A, Johnson C, et al. Prognostic importance of extensive coronary calcium on lung cancer screening chest computed tomography. CMAJ. 2024;196:E1362-9. doi:10.1503/cmaj.231602.
8. Mohajer B, Chernyak V. Reading between the lungs: coronary calcium at low-dose CT for lung cancer screening as a long-term prognostic marker. Radiology. 2025;316:e252713. doi:10.1148/radiol.252713.
9. Wang TW, Tzeng YH, Wu KT, Liu HR, Hong JS, Hsu HY, et al. Meta-analysis of deep learning approaches for automated coronary artery calcium scoring: performance and clinical utility. Comput Biol Med. 2024;183:109295. doi:10.1016/j.compbiomed.2024.109295.
10. Kim S, Park EA, Ahn C, Jeong B, Lee YS, Lee W, et al. Performance of fully automated deep-learning-based coronary artery calcium scoring in ECG-gated calcium CT and non-gated low-dose chest CT. Eur Radiol. 2025;35:7084-95. doi:10.1007/s00330-025-11559-4.
11. Perez-Cervera J, Arce J, Fattouh M, Kuno T, Schenone AL, Brahmanandam V, et al. Influence of BMI on virtual coronary artery calcium scoring. Int J Cardiovasc Imaging. 2023;39:863-72. doi:10.1007/s10554-022-02785-8.
12. Zhu Y. Non-gated chest CT for coronary artery calcium score: is this reliable? Eur Radiol. 2024;34:4457-8. doi:10.1007/s00330-023-10472-y.
13. Shin JM, Kim TH, Kim JY, Park CH. Coronary artery calcium scoring on non-gated, non-contrast chest computed tomography using wide-detector, high-pitch and fast gantry rotation: comparison with dedicated calcium scoring CT. J Thorac Dis. 2020;12:5783-93. doi:10.21037/jtd-20-1371.
14. Suh YJ, Kim C, Lee JG, Oh H, Kang H, Kim YH, et al. Fully automatic coronary calcium scoring in non-ECG-gated low-dose chest CT: comparison with ECG-gated cardiac CT. Eur Radiol. 2023;33:1254-65. doi:10.1007/s00330-022-09117-3.
15. Sudre CH, Li W, Vercauteren T, Ourselin S, Cardoso MJ. Generalised dice overlap as a deep learning loss function for highly unbalanced segmentations. In: Deep learning in medical image analysis and multimodal learning for clinical decision support. 2017. p. 240-8. doi:10.1007/978-3-319-67558-9_28.
16. Hecht HS, Blaha MJ, Kazerooni EA, Cury RC, Budoff M, Leipsic J, et al. CAC-DRS: coronary artery calcium data and reporting system—an expert consensus document of the Society of Cardiovascular Computed Tomography. J Cardiovasc Comput Tomogr. 2018;12:185-91. doi:10.1016/j.jcct.2018.03.008.
17. Zeleznik R, Foldyna B, Eslami P, Weiss J, Alexander I, Taron J, et al. Deep convolutional neural networks to predict cardiovascular risk from computed tomography. Nat Commun. 2021;12:715. doi:10.1038/s41467-021-20966-2.
18. Eng D, Chute C, Khandwala N, Rajpurkar P, Long J, Shleifer S, et al. Automated coronary calcium scoring using deep learning with multicenter external validation. NPJ Digit Med. 2021;4:88. doi:10.1038/s41746-021-00460-1.
19. Abdelrahman K, Shiyovich A, Huck DM, Berman AN, Weber B, Gupta S, et al. Artificial intelligence in coronary artery calcium scoring detection and quantification. Diagnostics (Basel). 2024;14:125. doi:10.3390/diagnostics14020125.

20. Almeida SO, Honoris L, Defranco A, Port S, Li D, Nasir K, et al. Reliability of CAC scoring on nongated compared with gated cardiac CT scans from MESA. JACC Cardiovasc Imaging. 2020;13:177-8. doi:10.1016/j.jcmg.2019.08.007.
21. van der Werf NR, Willemink MJ, Willems TP, Vliegenthart R, Greuter MJW, Leiner T. Influence of heart rate on coronary calcium scores: a multi-manufacturer phantom study. Int J Cardiovasc Imaging. 2018;34:959-66. doi:10.1007/s10554-017-1293-x.
22. Meng L, Cui L, Cheng Y, Wu X, Tang Y, Wang Y, et al. Effect of heart rate and coronary calcification on the diagnostic accuracy of dual-source CT coronary angiography in patients with suspected coronary artery disease. Korean J Radiol. 2009;10:347-54. doi:10.3348/kjr.2009.10.4.347.
23. Zhang Y, van der Werf NR, Jiang B, van Hamersvelt R, Greuter MJW, Xie X. Motion-corrected coronary calcium scores by a convolutional neural network: a robotic simulating study. Eur Radiol. 2020;30:1285-94. doi:10.1007/s00330-019-06447-7.
24. Risch F, Schwarz F, Kroencke T, Decker JA. Heart rate sensitivity of virtual non-contrast calcium scores derived from photon counting detector CT data: a phantom study. Radiol Med. 2024;129:401-10. doi:10.1007/s11547-024-01773-3.
25. Shim J, Kim K, Lee Y. Evidence-based investigation of coronary calcium score in cardiac computed tomography. Appl Sci. 2024;14:8906. doi:10.3390/app14198906.
26. Kang HW, Ahn WJ, Jeong JH, Suh YJ, Yang DH, Choi H, et al. Evaluation of fully automated commercial software for Agatston calcium scoring on non-ECG-gated low-dose chest CT with different slice thickness. Eur Radiol. 2023;33:1973-81. doi:10.1007/s00330-022-09143-1.
27. Kim C, Hong S, Choi H, Yoo WS, Kim JY, Chang S, et al. Impact of deep learning-based image conversion on fully automated coronary artery calcium scoring using thin-slice, sharp-kernel, non-gated, low-dose chest CT scans: a multi-center study. Korean J Radiol. 2025;26:759-70. doi:10.3348/kjr.2025.0177.
28. Klemenz AC, Beckert L, Manzke M, Lang CI, Weber MA, Meinel FG. Influence of deep learning based image reconstruction on quantitative results of coronary artery calcium scoring. Acad Radiol. 2024;31:2259-67. doi:10.1016/j.acra.2024.03.020.
29. Liu Y, Chen X, Liu X, Yu H, Zhou L, Gao X, et al. Accuracy of non-gated low-dose non-contrast chest CT with tin filtration for coronary artery calcium scoring. Eur J Radiol Open. 2022;9:100396. doi:10.1016/j.ejro.2022.100396.
30. Yu J, Qian L, Sun W, Nie Z, Zheng D, Han P, et al. Automated total and vessel-specific coronary artery calcium quantification on chest CT: direct comparison with CAC scoring on non-contrast cardiac CT. BMC Med Imaging. 2022;22:177. doi:10.1186/s12880-022-00907-1.
31. Becker J, Decker JA, Bette S, Braun F, Canalini L, Wollny C, et al. Impact of BMI, heart rhythm, and heart rate on photon-counting detector virtual coronary calcium scoring. Int J Cardiovasc Imaging. 2025;41:1331-9. doi:10.1007/s10554-025-03419-5.

Figures

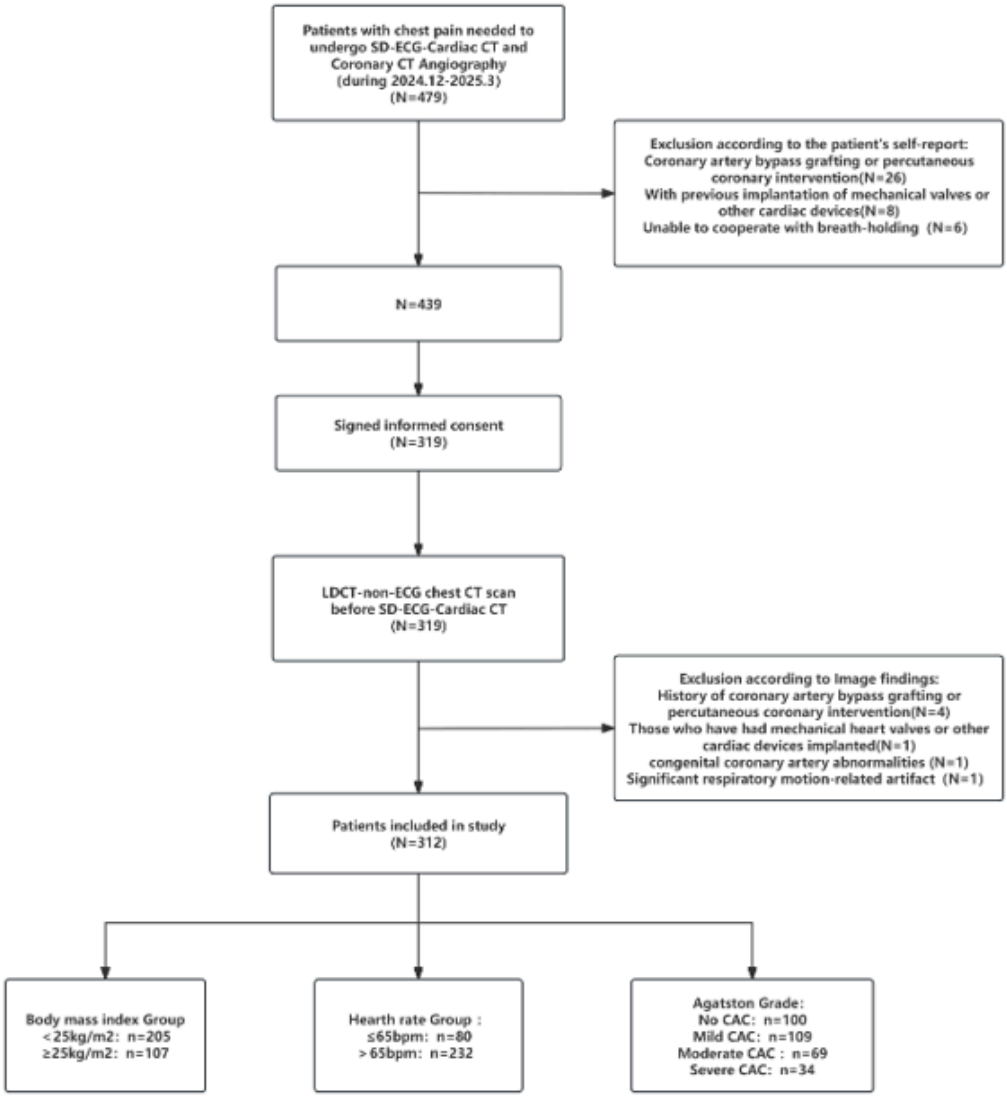


Figure 1

Study flowchart. The flow diagram shows specific admission criteria and grouping.

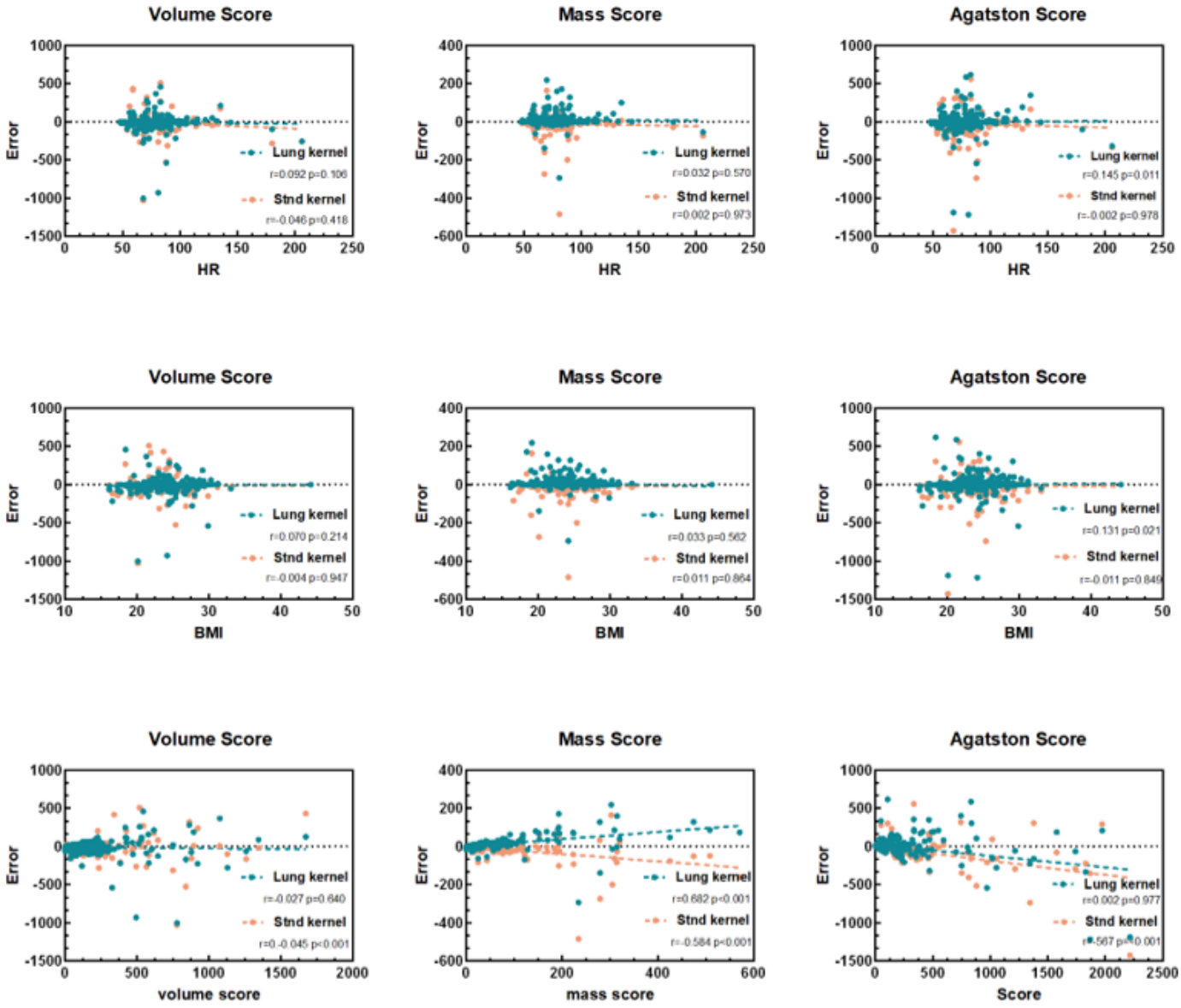


Figure 2

Error and Factor Correlation Analysis Chart. Error indicates the difference in CACS between non-gated LDCT and ECG-gated cardiac CT

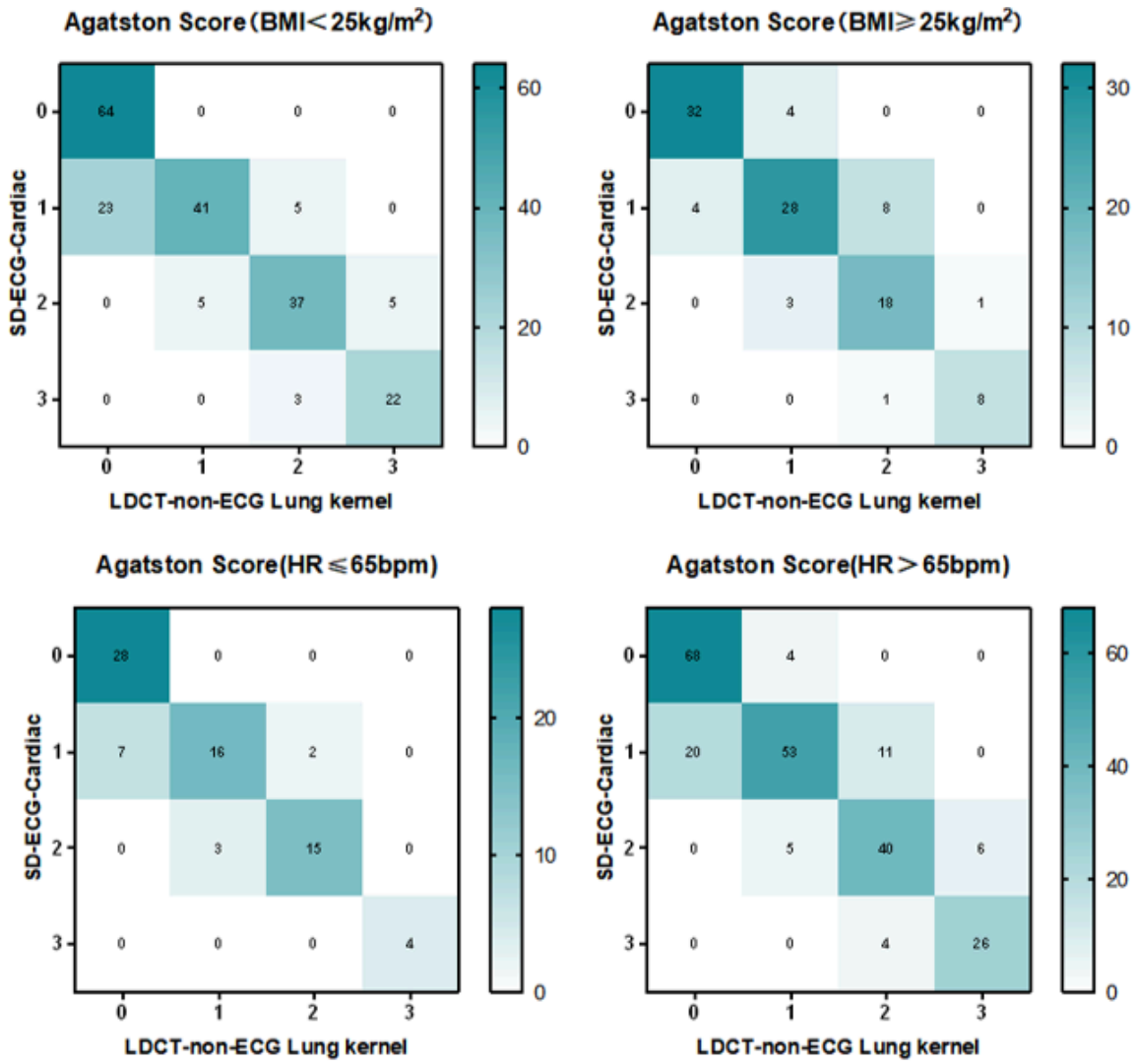


Figure 3

Confusion matrix diagram. Among them, the top left image is the low BMI subgroup, the top right image is the high BMI subgroup, the bottom left image is the low HR subgroup, and the bottom right image is the high HR subgroup.

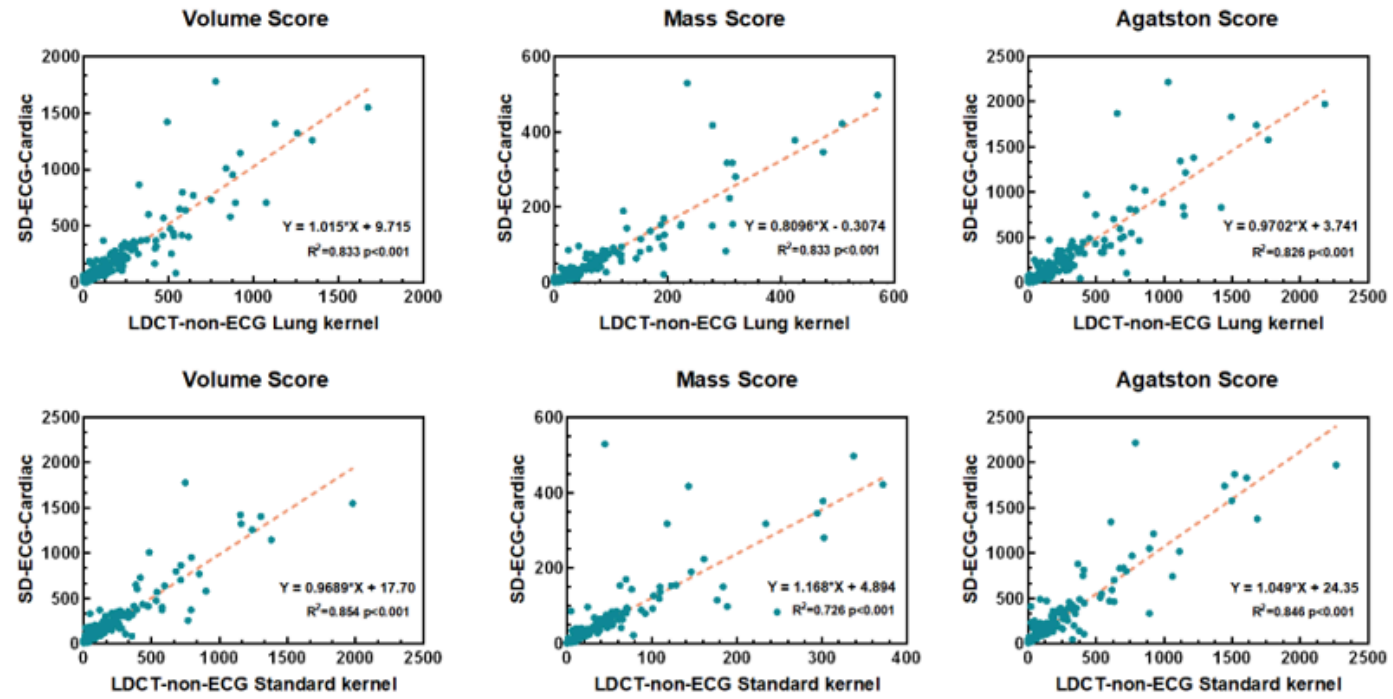


Figure 4

Linear correlation analysis chart

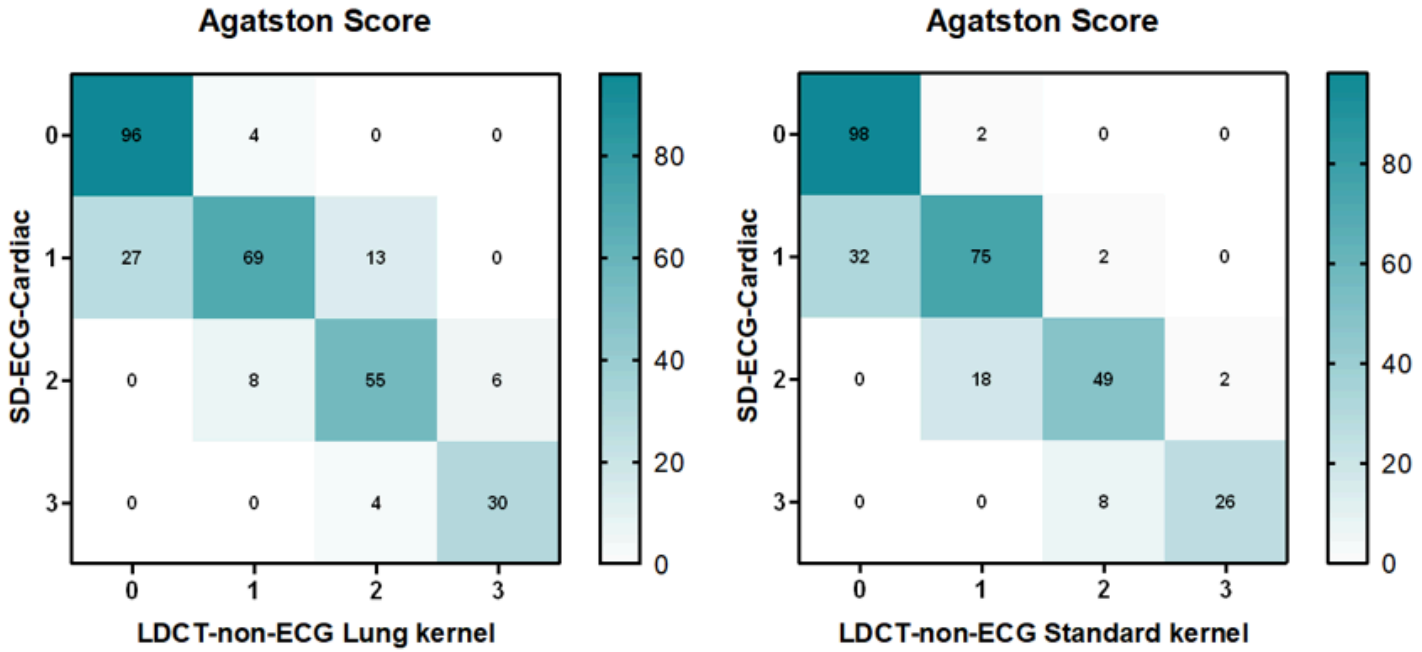


Figure 5

Confusion matrix diagram.